

In Situ Immobilization of Lead Species in Combustion Environments by Injection of Gas Phase Silica Sorbent Precursors

PRATIM BISWAS*^{·†} AND
MICHAEL R. ZACHARIAH[‡]

Aerosol and Air Quality Research Laboratory, Department of Civil and Environmental Engineering, University of Cincinnati, Cincinnati, Ohio 45221-0071, and Process Measurement Division, Chemical Sciences and Technology Laboratory, National Institute of Standards and Technology, Gaithersburg, Maryland 20899

A mechanistic study of the in situ immobilization of a toxic metal species in a high-temperature environment using gas phase sorbent precursors is described. Planar laser-based imaging measurements of fluorescence and particle scattering have been obtained to study the interaction of lead with silicon species in high-temperature oxidizing environments. The application of laser-induced fluorescence, the spectroscopy of PbO(g), and the techniques of measurement of gas phase precursors to particle formation are discussed. The silicon precursor is oxidized to form silica particles in the high temperatures, followed by a reactive scavenging of PbO(g). The result is that the lead oxide gas phase concentration is reduced, and homogenous nucleation of lead species is suppressed. The resultant particles are not only larger than a lead only case but also have morphologies in which lead is effectively immobilized and vitrified within a silica matrix. Trace quantities of silicon species have been shown to be effective in conversion of lead oxide to lead silicate. The measured conversion efficiencies of lead oxide to lead silicate agree well with equilibrium calculations, and no rate limitations were observed.

Introduction

Title III of the 1990 Clean Air Act Amendments stipulate the emission control of 11 toxic metals and their species. These metallic species are encountered in several combustion environments such as waste incinerators, coal combustors, and smelters. It has been well-established that these species are enriched in the submicrometer sizes in combustion exhausts (1). Moreover, particulate control devices have a minima in the collection efficiency in size ranges over which toxic metals are predominantly present. A potential method of controlling these metallic species emissions is by the use of sorbents. Several studies on metals capture by sorbents

have been conducted (2–6). Uberoi and Shadman (2) reported the use of various minerals such as alumina, bauxite, and kaolinite for capture of alkali metal, lead, and cadmium species. Scott et al. (5) reported the use of silica-based sorbents for capture of lead. Ho et al. (6) have reported the results of lead capture in a fluidized bed of sand. Extensive equilibrium calculations have been performed, and the results indicate that several silica, alumina, and titania compounds have the potential to form metallic complexes with species such as lead, selenium, mercury, arsenic, and chromium (7).

Sorbent injection into the combustion chamber provides for effective ways of chemisorbing metallic species. However, there are several physicochemical considerations that may hinder usage of bulk solid sorbents. Injection of bulk solid sorbents may result in the formation of outer layer metal–sorbent complexes that block the inner sorbent material from further chemisorbing metallic species (3). Specifically for lead capture using kaolinite, the complex has a lower melting point resulting in the formation of a glassy surface (5) that inhibits further chemisorption. Packed beds of sorbent materials also have to be maintained at optimal temperatures and may result in significant additional costs. A key factor to be noted is that coal combustors and incinerators have low concentrations of metallic species, and for sorbent systems to be cost-effective, excess sorbent materials should not be used. Moreover, studies indicate that, when large sorbent particles are used, the inner material is not effective due to pore pluggage. Alternate gas phase sorbent precursors for capture of trace metal species have been proposed by Owens and Biswas (8, 9). Such approaches provide an in situ means of capture of the toxic metal in the combustor environment and conversion to a benign form (low resultant leachability) and also suppress the homogeneous nucleation of the volatile metal species downstream of the combustion chamber. Detailed size distributions have been reported (8, 9), though there is a need to better understand the mechanisms of the metal–sorbent reactions.

In situ measurements for investigating the gas phase species' concentrations, temperature field, and particle size distributions can lead to a better understanding of the underlying chemical/transport phenomena. While conventional diagnostic tools such as thermocouples and mass/particle sampling probes have been used in the past, laser-based diagnostics offer non-intrusive, sensitive techniques for such measurements. Light scattering has been used extensively for measurement of particle size and number distributions in both aerosol and combustion research applications (for example, see refs 10 and 11). Laser-induced fluorescence (LIF) has been used extensively for gas phase concentration measurements in combustion environments (12). This technique is only recently being exploited in gas-particle conversion systems (13, 14).

In this paper, planar laser-based imaging measurements are used to provide in situ chemical information of a lead-silicon reaction system. Two-dimensional imaging of gas phase lead oxide (PbO) fluorescence is used to illustrate the reactivity of lead species with silica sorbents. A brief description of the application of LIF, the spectroscopy of lead oxide, and the experimental system is provided. The results of the measurements in a flame system (high temperature) and exit of a furnace reactor (two lower temperatures) are presented and discussed.

* To whom correspondence should be addressed; telephone 513-556-3697; fax: 513-556-2599; e-mail: pratim.biswas@uc.edu.

[†] University of Cincinnati.

[‡] National Institute of Standards and Technology.

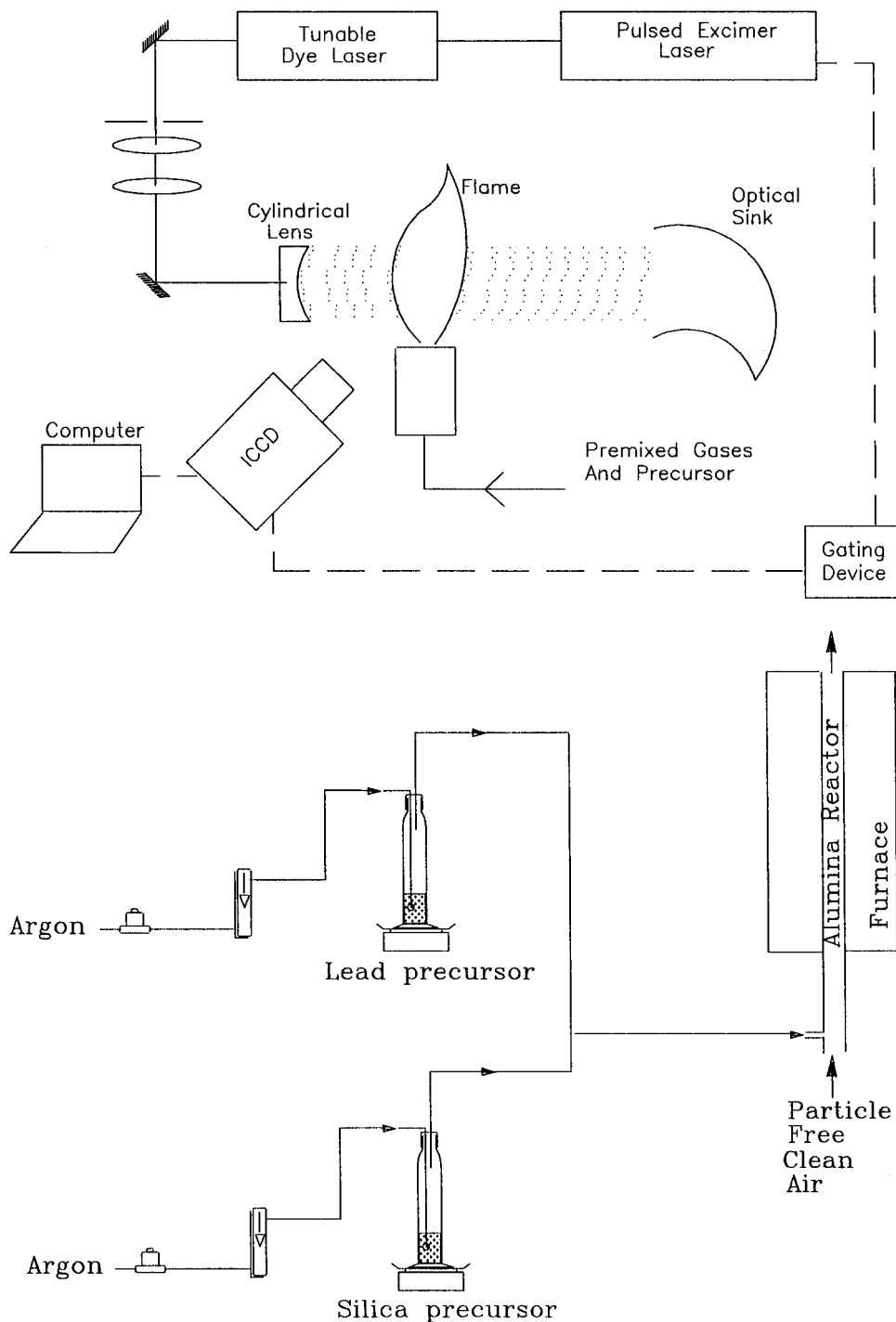


FIGURE 1. Schematic diagram of experimental system. (a) Premixed flame system; (b) furnace reactor system.

Experimental System and Plan

The schematic diagram of the experimental system is shown in Figure 1. Two different systems were used: a burner configuration (Figure 1a) and a furnace configuration (Figure 1b). The first set of experiments were carried out using a water cooled, premixed burner (diameter 8.7 mm) mounted on a vertical translation stage (14). Methane-oxygen flames with appropriate dilution using nitrogen was used to obtain a stable premixed flame. The lead precursor (tetraethyl lead) was entrained in an argon stream by bubbling and mixing with the fuel-oxidant mixture prior to introduction into the flame. This system was used to elucidate PbO spectroscopy and to obtain the laser-induced fluorescence characteristics. Experiments were then conducted with a co-feed of the silicon precursor (hexamethyldisiloxane) also entrained in an argon

stream by vapor saturation. The second set of experiments were conducted by using a furnace reactor (Figure 1b), with measurements made at the exit of the reactor (50 cm long, 7.5 mm diameter) as shown. The lead and silicon precursors were premixed with oxygen and nitrogen and inlet into the furnace reactor. The detailed operating conditions for the experiments are outlined in Table 1.

The laser excitation source for the experiments was a XeCl excimer-pumped dye laser, operating at 10 Hz with a 30-ns pulse duration, approximately 5 mJ pulse energy, and 0.2 cm^{-1} band width. For the initial spectroscopy measurements, the cylindrical beam was directed through the flame region and the fluorescent intensity monitored as a function of the incident wavelength (from 565 to 572 nm). A PMT was used to detect the fluorescent light intensities. To minimize

TABLE 1. Experimental Conditions

Flame System (Temperature = 2400 K, Figure 1a)									
case	reactant flow rates (L/min at 25 °C)			precursor feed rates (mol/s)		Pb:Si (molar ratio)			
	CH ₄	O ₂	N ₂	lead	silicon				
1	0.475	1.25	2.85	1.095×10^{-7}	0				
2	0.475	1.25	2.85	1.095×10^{-7}	4.99×10^{-7}	1:4.6			

Furnace System (Figure 1b)									
case	temperatures (K)			reactant flow rates (L/min at 25 °C)		precursor feed rates (mol/s)		Pb:Si (molar ratio)	
	maximum center	average (inside furnace)	final (35 mm from reactor exit)	O ₂	N ₂	lead	silicon		
3	1373	1270	980	1.25	2.85	1.095×10^{-7}	0		
4	1373	1270	980	1.25	2.85	1.095×10^{-7}	4.99×10^{-7}	1:4.6	
5	1373	1270	980	1.25	2.85	1.095×10^{-7}	1.1×10^{-6}	1:10	
6	1373	1270	980	1.25	2.85	1.095×10^{-7}	2.3×10^{-6}	1:20	
7	1223	1173	955	1.25	2.85	1.095×10^{-7}	0		
8	1223	1173	955	1.25	2.85	1.095×10^{-7}	4.99×10^{-7}	1:4.6	

contributions from scattering, a long pass filter (OG-590, Schott glass filter) was used to block light of wavelength less than 590 nm from being detected by the PMT. After selection of an excitation frequency (details in PbO spectroscopy section), a cylindrical and spherical lens combination was used to obtain a sheet beam that was directed over the measurement region as shown in Figure 1. The laser energy and its spatial distribution were monitored during the experiments by directing a 5% reflection of the laser sheet onto a dye cell and recording the intensity with a video CCD camera and frame grabber computer board. A line filter (Corion P10-530 nm) was used for the light scattering measurements (no fluorescence at 530 nm).

The images obtained were averaged over 250 laser shots to improve the signal to noise ratio and were spatially averaged 2×2 pixels, which is the effective resolution of the intensifier. All the image intensities were then corrected for camera dark background, flatfield uniform response of the camera and collection lens, and laser energy and spatial distribution. The fluorescence images were also corrected for laser-induced particle incandescence and scattering by subtracting images obtained with the laser detuned from the absorption transition. The flatfield correction was obtained by imaging uniform light from a standard, diffuse tungsten lamp through the appropriate spectral filters for fluorescence or particle scattering. As mentioned above, the video CCD images of laser-induced fluorescence from a static cell of dilute Rhodamine 590 dye in methanol were used to normalize the laser energy and vertical spatial distribution in the corrected images. The laser profile images were remapped from the video CCD to the intensified CCD coordinates based on images obtained with the laser sheet masked.

PbO Spectroscopy

There have been several reports on the spectroscopy of lead oxide in the literature. High-resolution absorption studies of PbO have been reported by Shawhan and Morgan (15) and Barrow et al. (16). High-resolution emission studies of PbO have been reported by Christy and Blomenthal (17) and Ram et al. (18). The techniques of gas chemiluminescence and laser-induced fluorescence have been used by Oldenberg et al. (19) to identify a series of 55 bands in the 450–850-nm range. Several new bands of the chemiluminescent spectra of PbO were reported by Linton and Broida (20), primarily for the $A0^+ - X0^+$ transitions. The only study reporting the laser excitation spectrum of PbO was by Brom and Beattie (21). A flashlamp-pumped tunable dye laser was used to investigate the a-X band system of PbO. Dorko and co-workers (22) have characterized the chemiluminescence from electronically excited lead oxide. Martin et al. (23) report a

high-resolution Fourier transform spectroscopy of the PbO molecule and have reported the spectroscopic constants for a variety of transitions.

PLIF (planar laser-induced fluorescence) is a well-established spectroscopic flow diagnostic that is based on the spontaneous radiative emission (fluorescence) following absorption of laser photons by a specific molecular species. The theory and application of laser-induced fluorescence spectroscopy has been described in detail elsewhere (12–14). A detailed study of the fluorescence–excitation detection scheme for PbO was carried out and has been described in detail elsewhere (24). The $A^3\Pi(0^+) - X^1\Sigma^+(0^+)$ (0,3) excitation and associated transitions was used in this work. The partial excitation frequency spectrum obtained by scanning the laser from 567.5 to 571.5 nm in steps of 0.001 nm is shown in Figure 2. Using the spectroscopic constants reported by Oldenberg et al. (19), the synthetic spectra were calculated for the above-mentioned transition, and rotational line assignments made (Figure 2). The absorbing species concentration generally requires knowledge of the local collisional quenching rate coefficient and temperature. One strategy that is used is to assume a constant quenching rate (13, 14) and an absorption transition that is insensitive to temperature. Over the temperature range of interest in the flame (1800–2400 K), the net population of the Q (30) line (corresponding to a 569.32 nm excitation) varied by only 10% (24). Over the temperature range of 1000–1200 K (furnace experiments), the net population varied by 35%. Using these approximations, the fluorescence signal is a direct representation of the relative PbO(g) concentration in the flame.

Results and Discussion

Two systems, flame and furnace, were used to examine capture characteristics over a wide range of temperatures. The experimental conditions for all the different cases are listed in Table 1.

Flame System. The first set of experiments were carried out in a premixed flame environment where the temperature was approximately 2400 K. The lead oxide gas phase concentration image along with the elastic light scattering image (to a distance of 50 mm from the burner exit) for the two conditions, a lead only feed (case 1) and a lead–silicon precursor co-feed (case 2) are shown in Figure 3. The regions of high lead oxide vapor concentrations occur close to the flame front, and the concentration decreases (yellowish color, Figure 3a) downstream as the vapors begin nucleating and are converted to the particulate phase. However, we were unable to detect any scattered light in the downstream region along the centerline (white region), indicating that the particles were very small. The particles were only detectable

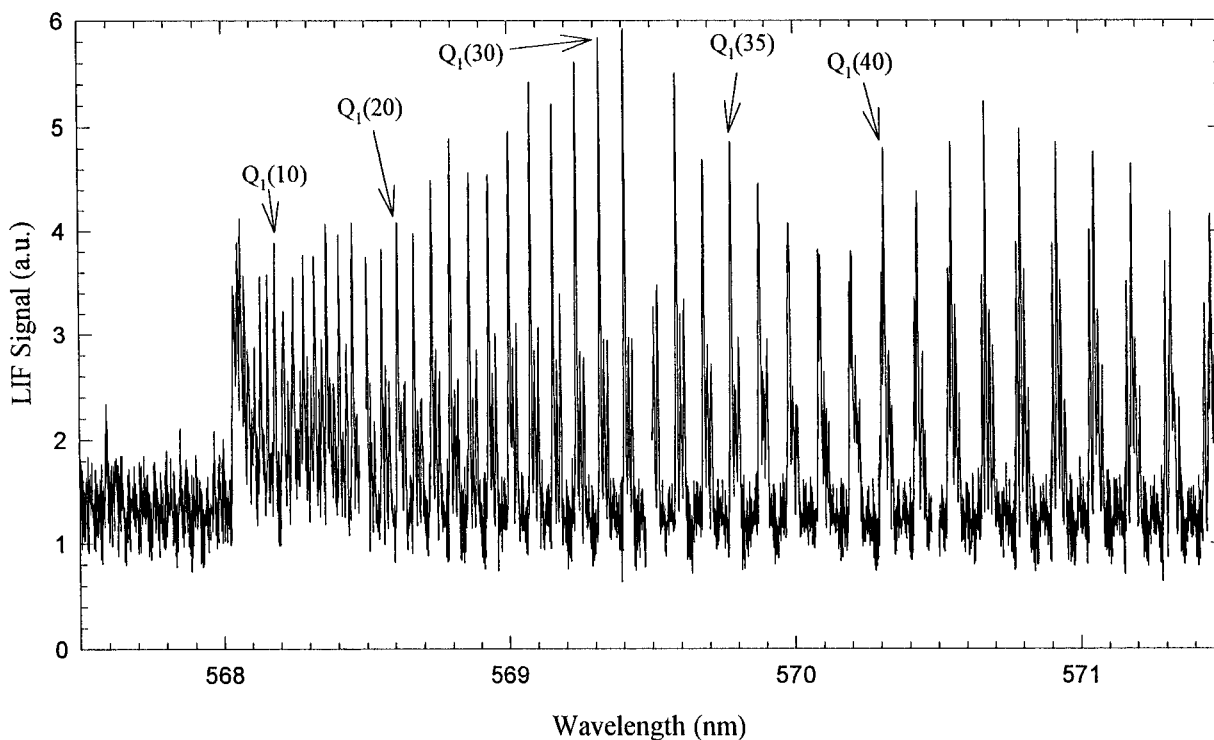


FIGURE 2. Laser excitation spectrum of PbO between 567.5 and 571.5 nm established with a resolution of 0.001 nm. Also shown are rotational states for a few lines.

in the peripheral regions (reddish yellow color), presumably due to the lower temperatures that promote a higher nucleation rate and the longer residence times allowing for growth of particles to larger sizes. When the silicon precursor is added with the lead feed, the high intensity of scattered light indicates that silica particles are formed and grow rapidly in the high-temperature regions, as confirmed with experiments with a silicon precursor feed only (14). These particles provide a surface for the condensation of lead vapors followed by chemical reaction, resulting in a lower gas phase PbO concentration (compared to case 1 with a lead only feed). Particles were also collected and analyzed by infrared spectroscopy (9) and Raman spectroscopy (25) and indicated a mix of lead silicate and silica particles, confirming that reactive scavenging was taking place.

The system can be modeled to predict the size distribution of the resultant metal-sorbent composite. Discrete sectional models (26) allow for the accurate modeling of early stages of particle formation (27) and are used in this work. The centerline PbO(g) concentration data obtained from the PLIF images (Figure 3a, by scaling the peak concentration to the molar feed rate) is plotted in Figure 4 for the lead only (case 1) and lead and silicon precursor co-feed (case 2). Also shown are predictions of a discrete sectional model (28). A brief description is provided here, and the reader is referred to earlier papers for the model development and application (27, 28). First, the reactants are oxidized to form the PbO and SiO monomers, and their rate of formation is expressed using the first-order rate constants, $k_{1,Pb}$ and $k_{1,Si}$. The values of these rate constants are obtained from the literature as described by Wu and Biswas (28). The monomers then form dimers, and the dimer formation rates for lead oxide and silicon oxide are expressed using the second-order rate constants, $k_{2,Pb}$ and $k_{2,Si}$, respectively. The value of $k_{2,Si}$ is obtained by molecular modeling computations reported by Zachariah and Tsang (29). No kinetic constant for PbO dimer formation was available in the literature, and hence the measurements for the lead only feed (case 1) were used to fit to the model predictions to find $k_{2,Pb}$. Brownian coagulation expressions were used to calculate the larger cluster formation

rates. Using the rate constant values described above, the model predictions were compared to the centerline measurements for case 2 (co-feed of silicon and lead), and good agreement (Figure 4) was obtained using an accommodation factor, $a = 0.01$, to account for the condensation of lead oxide onto a silica surface. This is consistent with reports in the literature that collisions among different species are imperfect (30). A more detailed description on the determination of the accommodation factor is provided by Wu and Biswas (28). An overall decrease of 25% in PbO(g) concentration was obtained (with the silicon precursor co-feed), which is substantially higher than that predicted by equilibrium calculations (Figure 8).

Furnace Experiments. The second set of measurements were carried out at the exit of a furnace reactor (cases 3–8, at lower temperatures than the flame system, tabulated in Table 1) for different ratios of Pb:Si. The PLIF images are shown in Figure 3b for Pb:Si ratios of 1:0, 1:4.6, and 1:10. The lead oxide vapor concentration is highest at the exit of the reactor (red region) and decreases downstream (yellow) as the temperature decreases and the vapor is converted to particles. The concentration of PbO(g) at the exit of the furnace (lowest point in the image) is progressively lower (lighter colors) as more of the PbO(g) is scavenged with increasing amounts of silicon precursor feed. Unlike the flame experiments, however, PbO(g) concentrations reach much lower values, indicating more effective scavenging at these lower temperatures (relative to those in the flame).

The normalized (by the PbO(g) concentration at $x = 12.5$ mm for a lead only feed at the set temperature) centerline PbO(g) concentration is plotted as a function of distance from the reactor outlet in Figure 5. For the lead only precursor feed cases (3 and 7), lead oxide vapors are formed in the furnace by precursor oxidation. We infer that the lead is primarily present as gas phase lead oxide at the exit as no particles could be detected by light scattering measurements at the outlet of the furnace reactor, consistent with equilibrium calculations (31). Further downstream the lead oxide concentration decreases due to conversion to particles by nucleation. The drop in the lead oxide gas phase concentra-

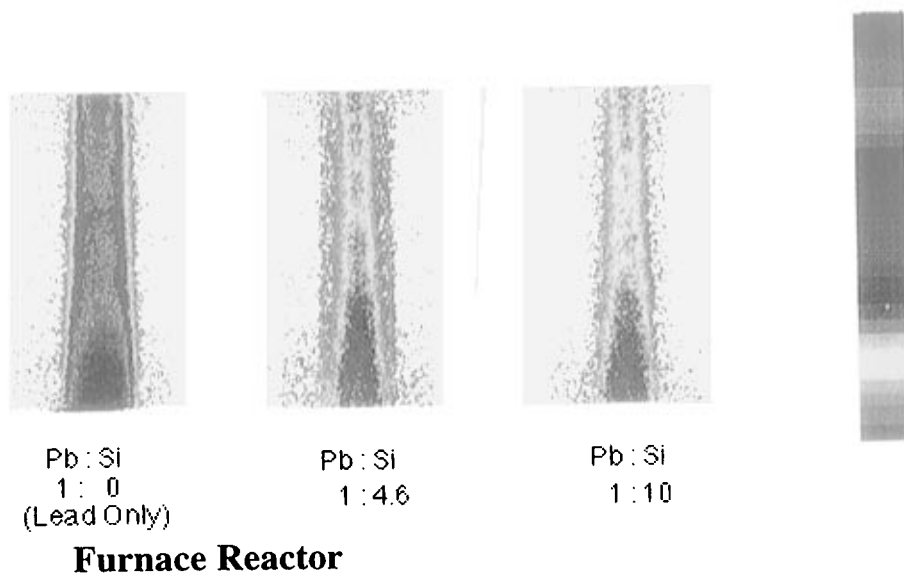
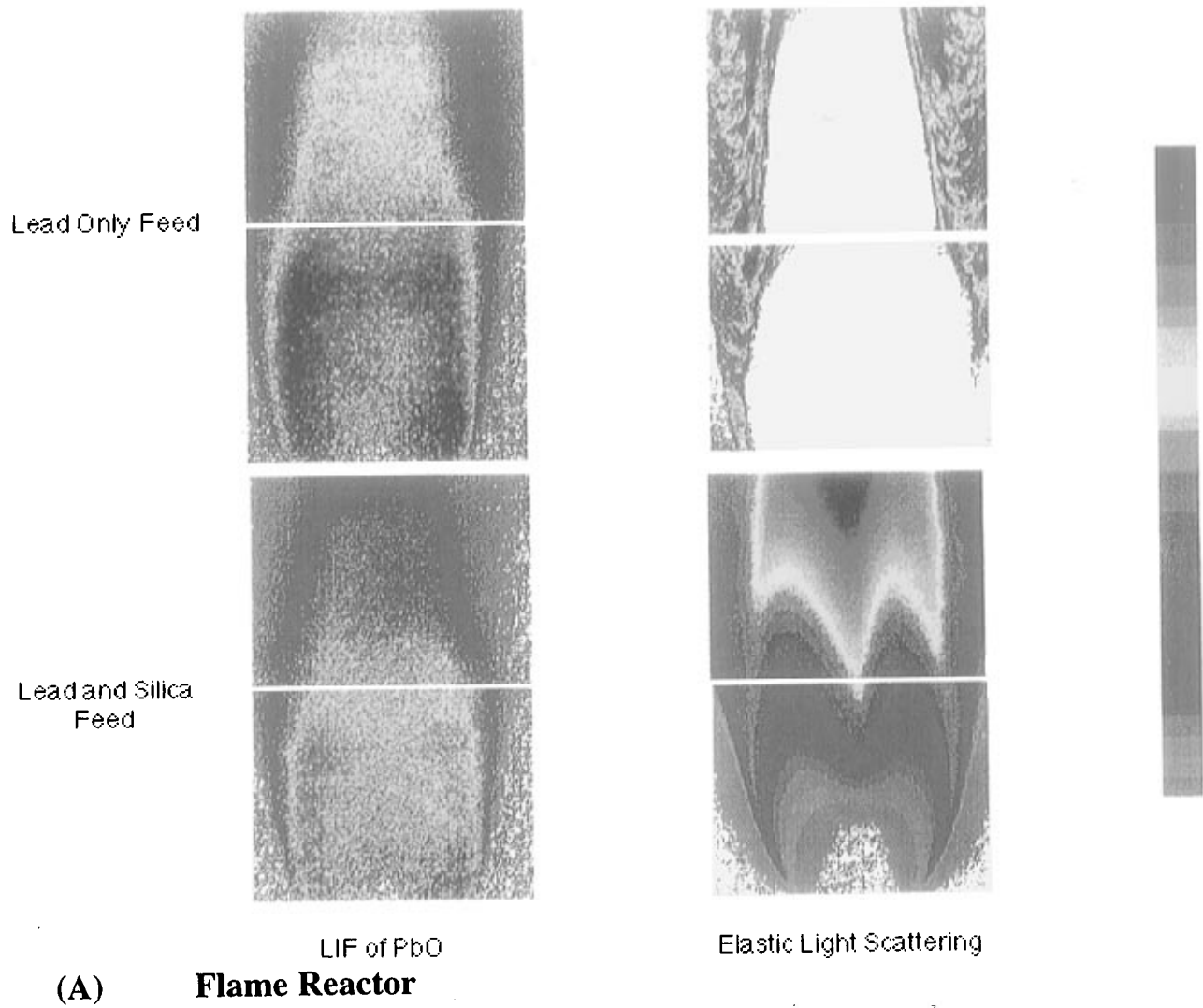


FIGURE 3. (A) Two-dimensional images at the exit of the flame reactor illustrating LIF images for a lead only feed (case 1) and a co-feed of lead and silica precursor (case 2). Also shown on the right are the corresponding light scattering images. The color bar indicates increasing concentrations of PbO(g) and light scattering intensities from bottom to top. (B) Two-dimensional images at the exit of the furnace reactor illustrating LIF images for a lead only feed (case 3) and a co-feed of lead and silica precursor at ratios of 1:4.6 (case 4) and 1:10 (case 5). The color bar indicates increasing concentrations of PbO(g) from bottom to top.

tion is faster for case 7 as compared to case 3 due to the lower temperatures, which result in a higher particle formation rate. The lead oxide concentration reaches a final steady value

(equilibrium with particles at the corresponding temperature). This ratio of the concentrations for cases 3 and 7 is approximately 2.44 (Figure 5) and close to the computed ratio

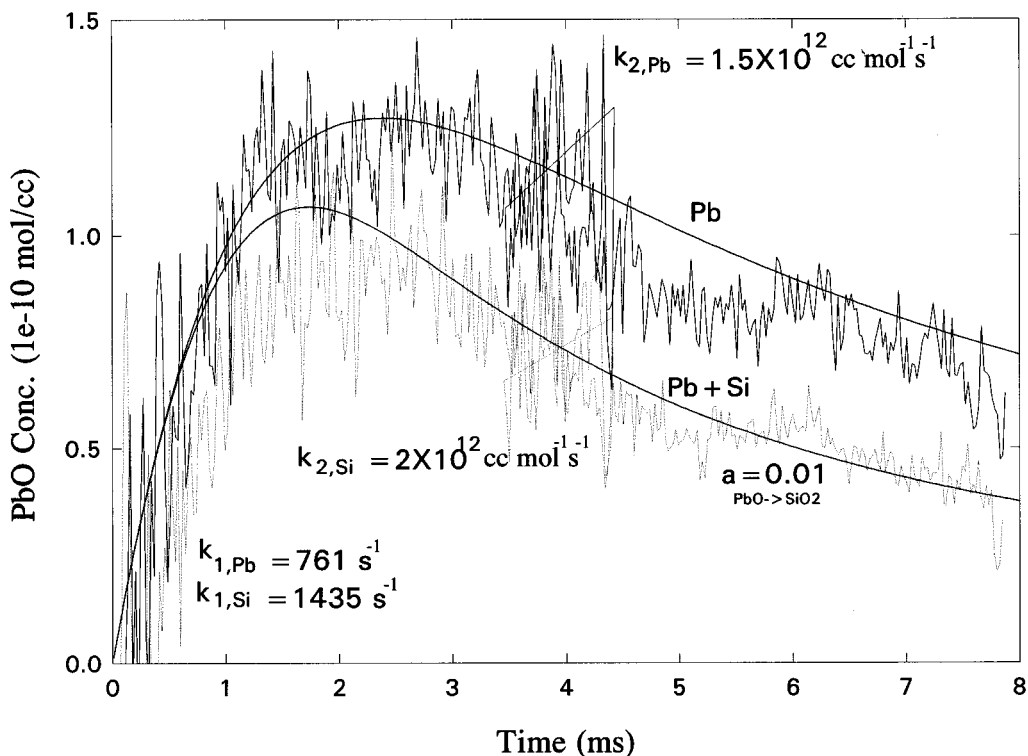


FIGURE 4. Centerline profile of PbO(g) concentration as a function of time from the flame front for a lead only feed rate (case 1) and lead-silicon co-feed (case 2).

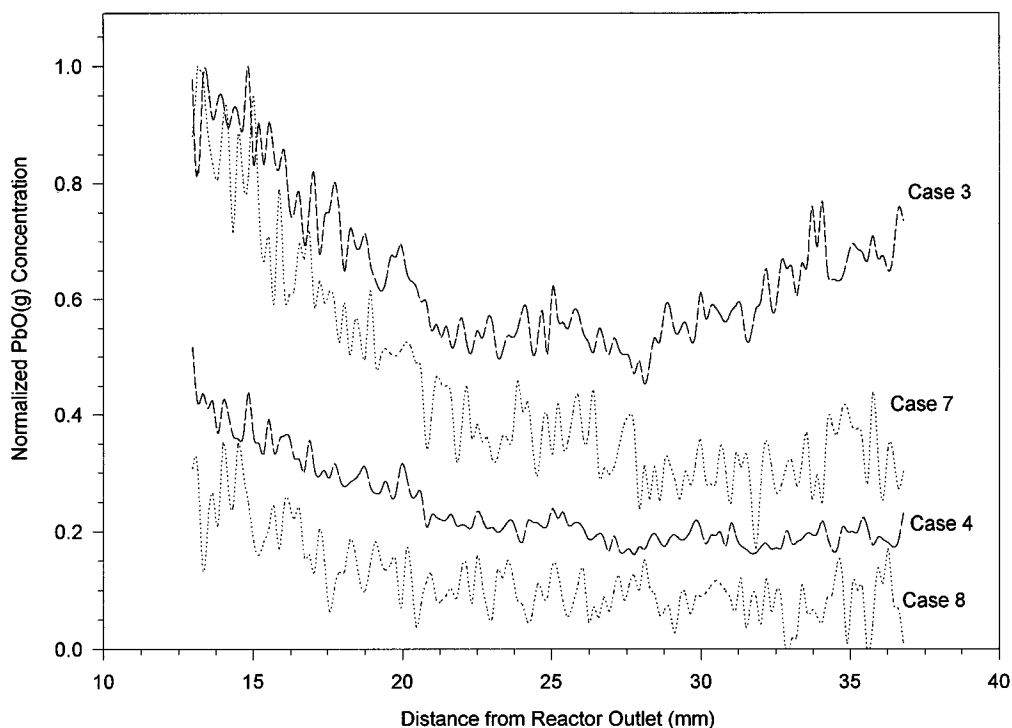


FIGURE 5. Centerline profile of normalized (by concentration at exit of furnace for a lead only feed) PbO(g) concentration for the furnace experiments as a function of distance from the exit of the reactor for cases 3, 4, 7, and 8.

of 2.2 assuming equilibrium conditions (saturation pressure of PbO at the final temperature listed in Table 1). The normalized concentration at a distance of 35 mm is also close to the predicted equilibrium ratios (PbO(g)/PbO(condensed)) at the two temperatures of 980 and 955 K.

On comparing the performance of a lead only feed (cases 3 and 7) to a lead and silicon precursor co-feed (cases 4 and 8), the following observations can be made. First, the concentration of PbO(g) at the outlet of the reactor is lower

due to some of it being scavenged by the silica particles inside the furnace (silica particles are formed in the high-temperature zone as illustrated earlier). The removal efficiency of lead oxide inside the furnace for case 4 is approximately 60% (estimated by $1 - \text{the ratio of the PbO(g) centerline concentrations from Figure 5 at } x = 12.5 \text{ mm for cases 4 and 3}$) and close to the value of 58% obtained by equilibrium computations at 1270 K (7). For case 8, the removal efficiency is 75%, compared to the computed value of 68% at 1170 K.

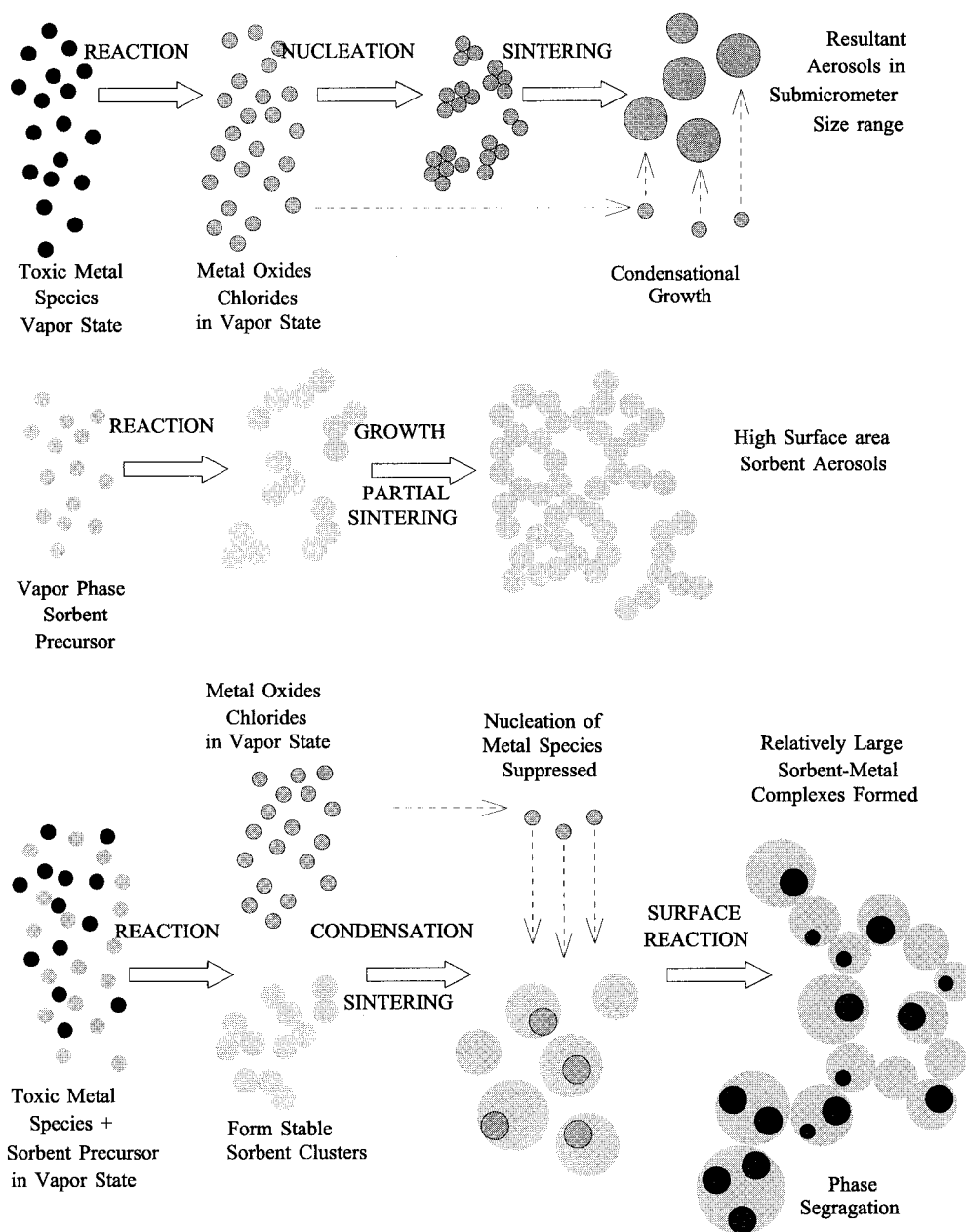


FIGURE 6. Mechanistic representation of the lead-silicon reaction system.

The measured efficiencies agree with the equilibrium predictions at these residence times, confirming that there are no rate limitations. The residence time (approximately 70 ms) in the furnace is long enough to allow for transport of the lead oxide vapor to the silica surface and undergo complete reaction. Second, the concentration of $\text{PbO}(g)$ at the outlet of the reactor further decreases with distance. After a distance of 25 mm from the exit of the reactor, the $\text{PbO}(g)$ concentration reaches steady values. Analysis of the particles collected at this location indicate that there is no crystalline lead oxide in the sample, and infrared and Raman spectroscopy clearly indicates that the lead is bonded with the silica to form a lead silicate compound (9, 25). Electron microscopy with EDAX also illustrates that the lead is associated with the silica particles (9). These clearly indicate that nucleation of the lead oxide vapors (observed in cases 3 and 7, lead only feed) is suppressed in the presence of the silica particles. The overall removal efficiency of lead oxide for case 4 is 80% and for case 8 is 92%. The corresponding removal efficiencies as established by equilibrium calculations (7) are 82% and 90%, respectively, at the final temperature (35 mm from furnace reactor tube exit) listed in Table 1.

Mechanistic Interpretation and Implications. The gas phase behavior of PbO described above in conjunction with previous real time aerosol measurements (8, 9) provide sufficient detail to develop a mechanistic understanding of the process (Figure 6). At the high-temperature oxidizing environments, lead is primarily present in the gas phase as lead oxide. When a silicon precursor is co-fed, high surface area agglomerates of silica particles formed at high temperatures provide a site for reactive scavenging of gas phase lead oxide. This reduction in the gas phase PbO concentration results in a smaller quantity of lead oxide particles that can be formed by nucleation as the temperature decreases downstream. In summary, gas phase lead oxide is rapidly formed in the high-temperature regions, followed by a transport to the active silica surfaces and chemical reaction to form lead silicates. The transmission electron micrograph (Figure 7) of a resultant particle clearly confirms that the lead species is trapped in a silica matrix. Energy dispersive X-ray analysis, infrared, and Raman spectroscopy clearly indicate that the lead species is primarily present as a lead-silicon complex (9, 25).

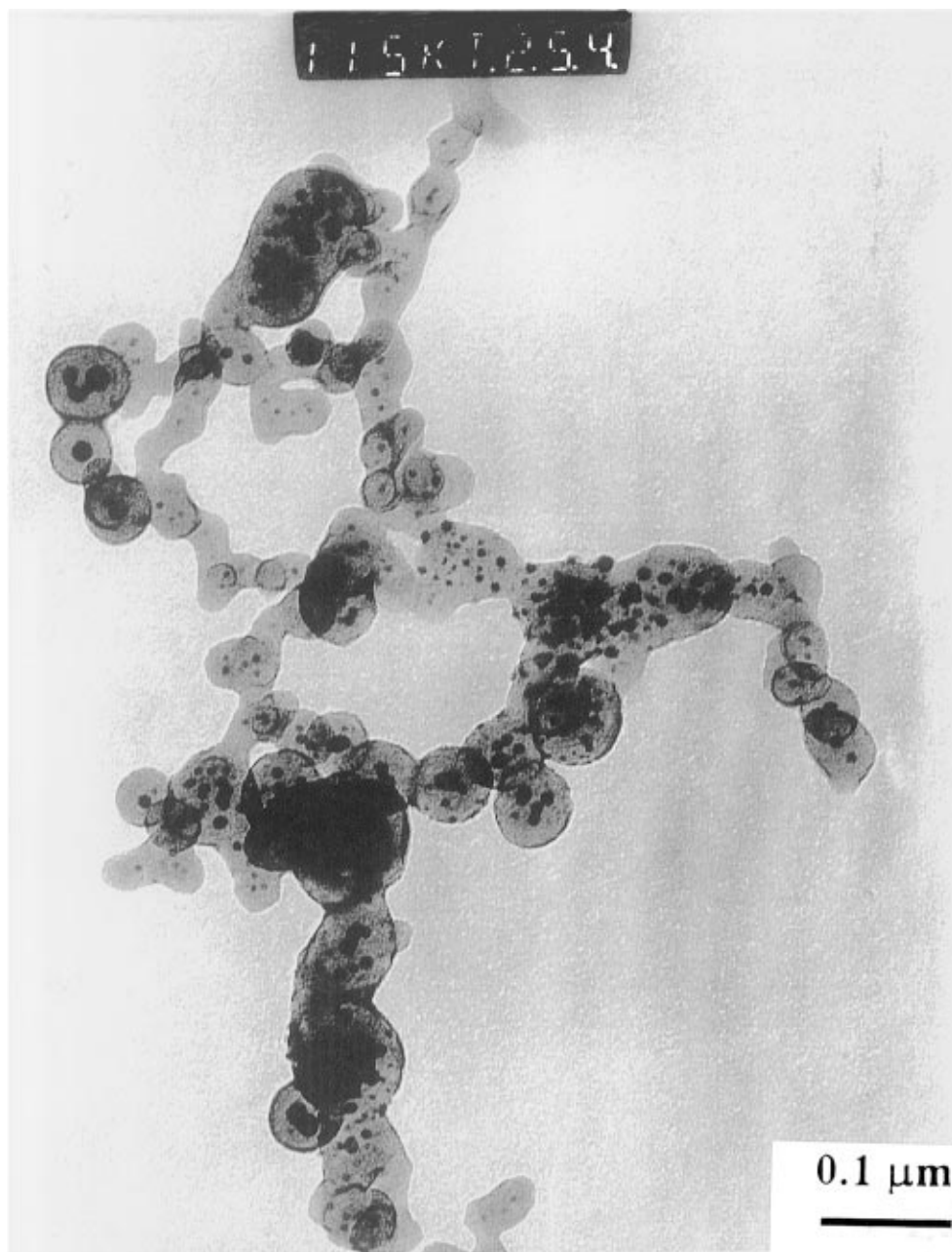


FIGURE 7. Transmission electron micrograph of the resultant lead-silica composite particles formed. The dark regions are the lead silicate compound dispersed in a silica matrix.

The removal efficiency (calculated from Figure 5 at the outlet of the reactor ($x = 12.5$ mm) and the final measurement position ($x = 35$ mm)) of the lead species at various temperatures with the corresponding values predicted by equilibrium calculations is plotted in Figure 8. As shown in Figure 8a, the lead capture efficiency is very sensitive to the temperature and mimics that predicted by equilibrium. Clearly for the residence times (70–100 ms) used in the furnace experiments, the chemistry is not kinetically controlled. At high temperatures, the capture efficiency in the flame is somewhat lower than that predicted by equilibrium. Because of the high temperatures, however, our confidence in the temperature measurement is not great as that for the flow reactor, and this may be one reason for the discrepancy. Alternatively, the flame has residence times (less than 10 ms) considerably shorter than the furnace reactor (70–100 ms), and the result may indicate a kinetically controlled regime. We are unable at this time to resolve this point, and further work is needed to clearly identify the onset of a kinetically controlled regime. The experimental results clearly indicate

that there is an optimal temperature range for lead species capture. At the higher temperatures, the reverse reaction (silicate decomposing to lead oxide and silica) is dominant. As the temperature is lowered to close to approximately 1000 K, the scavenging efficiency increases as the lead oxide-silica reaction resulting in the formation of lead silicate is dominant. Shown in Figure 8b is the effect of the silicon loading on the capture efficiency. Quite clearly surface area effects are not important, implying again that these are not kinetically (surface area or mass transfer) controlled processes. Presumably, this latter result is due to the nature of the co-injection in which very fine silica particles are being formed simultaneously with the lead and is one of the advantages of this process. Introducing the sorbent as a gas phase precursor alleviates the problem of pore plugging and solid phase mass transfer resistance encountered when bulk sorbents are used.

The potential of in situ generated sorbents for metals capture is evident from this work. First, a highly networked agglomerate of very high surface area silica particles is formed at combustor temperatures. The metallic species undergo

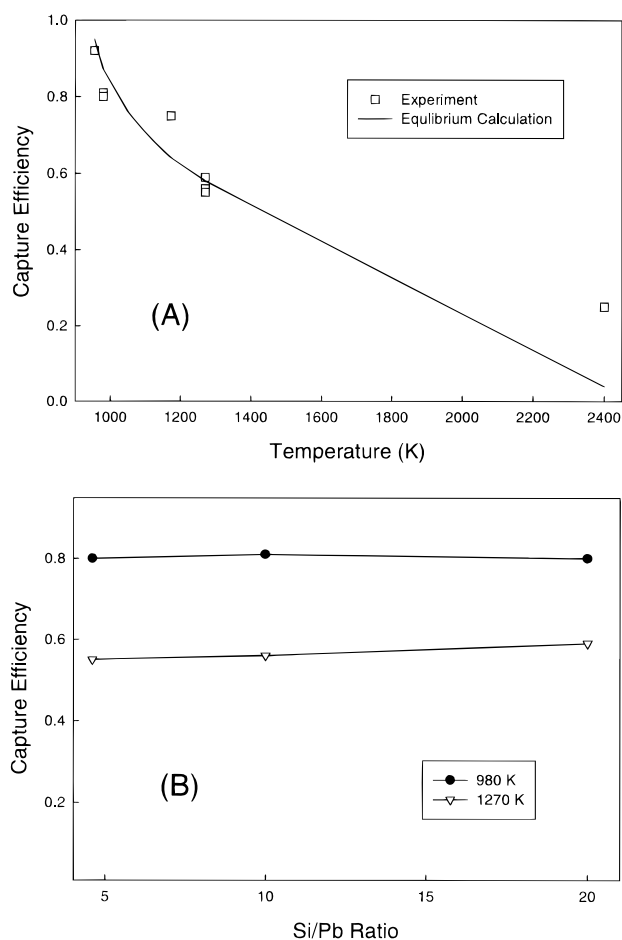


FIGURE 8. (A) Capture efficiency of lead species as a function of temperature. Symbols represent the experimental data, and the line represents the results of an equilibrium calculation. (B) Capture efficiency of the lead species as a function of the Si/Pb ratio at two temperatures. The symbols represent the experimental data, and the lines represent the results of equilibrium computations.

various reactions and intermediate oxide species are typically formed in the gas phase. As the sorbent oxide has a high affinity for the gas phase metal oxide, these are effectively scavenged, the effectiveness being highest at an optimal temperature (encountered as the gases traverse down the combustor). As the metal species are effectively removed from the gas phase, sufficient quantities are not present to nucleate and form the ultrafine mode of the aerosol, which is difficult to capture. Relatively low ratios of sorbent to metal have been shown to be effective for high capture efficiencies.

Acknowledgments

Partial support was provided by the Chemical Sciences Technology Laboratory, NIST, the U.S. Department of Energy (Grant DE-FG22-95PC95222), and the Ohio Coal Research Consortium (Grant OCRC 96-4.13). The authors also acknowledge the assistance of Brian McMillin and Maria Aquino in conducting the experiments; the assistance of Jim Maslar, NIST, in identification of the products by Raman spectroscopy; and the fruitful discussions with C. Y. Wu and T. M. Owens, University of Cincinnati. This work was done while P.B. was on sabbatical at NIST.

Literature Cited

- (1) Linak, W. P.; Peterson, T. W. *24th Combustion (International) Symposium*; The Combustion Institute: Pittsburgh, 1986; p 399.
- (2) Uberoi, M.; Shadman, F. *AIChE J.* **1990**, *36*, 1433.
- (3) Uberoi, M.; Shadman, F. *Environ. Sci. Technol.* **1991**, *25*, 1285.

- (4) Wu, B.; Jaanu, K. K.; Shadman, F. *Environ. Sci. Technol.* **1995**, *29*, 1660.
- (5) Scotto, M. V.; Peterson, T. W.; Wendt, J. O. L. *2nd International Congress on Toxic Combustion ByProducts*; Salt Lake City, UT, 1992.
- (6) Ho, T. C.; Chen, C.; Hopper, J. R.; Oberacker, D. A. *Combust. Sci. Technol.* **1992**, *85*, 1001.
- (7) Owens, T. M.; Wu, C. Y.; Biswas, P. *Chem. Eng. Commun.* **1995**, *133*, 31.
- (8) Owens, T. M.; Biswas, P. *Ind. Eng. Chem. Res.* **1995**, *35*, 792.
- (9) Owens, T. M.; Biswas, P. *J. Air Waste Manage. Assoc.* **1996**, *46*, 530.
- (10) Zachariah, M. R.; Chin, D.; Semerjian, H. G.; Katz, J. L. *Appl. Opt.* **1989**, *28*, 530.
- (11) Willeke, K.; Baron, P. *Aerosol Measurement, Techniques and Applications*; Van Nostrand Reinhold: New York, 1993; Chapter 32.
- (12) Eckbreth, A. C. *Laser Diagnostics for Combustion Temperature and Species*; Abacus Press: Cambridge, MA, 1988.
- (13) Zachariah, M. R.; Burgess, D. R. F. *J. Aerosol Sci.* **1994**, *25*, 487.
- (14) McMillin, B.; Biswas, P.; Zachariah, M. R. *J. Mater. Res.* **1996**, *11*, 1552.
- (15) Shawhan, E. N.; Morgan, F. *Phys. Rev.* **1935**, *47*, 377.
- (16) Barrow, R. F.; Deutsch, J. L.; Travis, D. N. *Nature* **1961**, *191*, 374.
- (17) Christy, A.; Blomenthal, S. *Phys. Rev.* **1930**, *35*, 46.
- (18) Ram, R. S.; Singh, J.; Upadhyaya, K. N. *Spectrosc. Lett.* **1973**, *6*, 515.
- (19) Oldenberg, R. C.; Dickson, C. R.; Zare, R. N. *J. Mol. Spectrosc.* **1973**, *58*, 283.
- (20) Linton, C.; Broida, H. P. *J. Mol. Spectrosc.* **1976**, *62*, 396.
- (21) Brom, J. M.; Beattie, W. H. *J. Mol. Spectrosc.* **1980**, *81*, 445.
- (22) Dorko, E. A.; Glessner, J. W.; Ritchey, C. M.; Rutger, L. L.; Pow, J. J.; Brasure, L. D.; Duray, J. P.; Snyder, S. R. *Chem. Phys.* **1986**, *102*, 349.
- (23) Martin, F.; Bacis, R.; Verges, J.; Bachar, J.; Rosenwaks, S. *Spectrochim. Acta* **1988**, *44*, 889.
- (24) Biswas, P.; Yang, G.; Zachariah, M. R. *Combust. Sci. Technol.* In press.
- (25) Maslar, J.; Biswas, P.; Zachariah, M. R. Raman Spectra of Lead-Silica Complexes Formed in High Temperature Environments, unpublished work, 1994.
- (26) Wu, J. J.; Flagan, R. C. *J. Colloid Interface Sci.* **1988**, *123*, 339.
- (27) Biswas, P.; Wu, C. Y.; Zachariah, M. R.; McMillin, B. *J. Mater. Res.* **1997**, *12*, 714.
- (28) Wu, C. Y.; Biswas, P. Study of Numerical Diffusion in a Discrete Sectional Model and Its Application to Aerosol Dynamics Simulation. *Aerosol Sci Technol.* In press.
- (29) Zachariah, M. R.; Tsang, W. *J. Phys. Chem.* **1995**, *99*, 5308.
- (30) Ulrich, G. D.; Riehl, J. W. *J. Colloid Interface Sci.* **1982**, *87*, 257.
- (31) Wu, C. Y.; Biswas, P. *Combust. Flame* **1993**, *93*, 31.

Received for review January 28, 1997. Revised manuscript received May 22, 1997. Accepted May 30, 1997.®

ES9700663

® Abstract published in *Advance ACS Abstracts*, July 15, 1997.